RSC Sustainability

ROYAL SOCIETY OF CHEMISTRY

PAPER

View Article Online
View Journal | View Issue

Cite this: *RSC Sustainability*, 2023, **1**, 554

Upcycling of spent functional biocarbon adsorbents to catalysts for the conversion of C5/C6 carbohydrates into platform chemicals†

Haixin Guo, *[ab] Yuto Inoue,[b] Yukiya Isoda,[b] Tetsuo Honma [c] and Richard Lee Smith, Jr *[b]

Received 4th January 2023
Accepted 22nd February 2023

DOI: 10.1039/d3su00004d

rsc.li/rscsus

Upcycling of spent heavy metal functional carbon adsorbents for use in catalytic applications must be considered to avoid hazardous wastes and to develop circular economies. In this study, amino-Brønsted acid precursor functional biocarbons were prepared by the hydrothermal-ammonia carbonization of biomass and subsequent mechanochemical modification with L-cysteine. Mix ball-milling of hydrothermal-ammonia-carbonized solids with L-cysteine afforded biocarbon materials with three kinds of sites, namely amino-functional, Brønsted acid precursor, and metal ion binding. The adsorption of Ni^{2+} metal onto biocarbons was high (Q_m > 313 mg g^{-1}) and the spent adsorbents could be upcycled by the oxidation of Brønsted acid precursor sites (–SH groups) with H_2O_2 and applied as catalysts for C5/C6 carbohydrate dehydration–oxidation reactions. In an ionic liquid [BMIM]Cl reaction phase, the spent adsorbent catalyzed the conversion of C5 carbohydrate substrate xylose to furoic acid and furfural in yields of 46.2% and 24.7%, respectively, while C6 carbohydrate substrates, fructose and glucose, afforded 5-hydroxymethylfurfural in yields of 71% and 24%, respectively. The preparation procedure for amino-functional biocarbons allows heavy metal recovery from wastewater and upcycling of spent materials to catalysts for carbohydrate dehydration–oxidation reactions.

Sustainability spotlight

Advanced materials for the removal of heavy metals from aqueous bodies are necessary to maintain clean water (SDG6) and to prevent environmental contamination (SDG14–15); however, their production, processing, recycle and reuse have problematic material intensity issues. Herein, through collaboration between China and Japan (SDG17), we demonstrate the transformation of biomass-derived materials *via* ammonia-water treatment and subsequent ball-milling with amino acids for producing functional biocarbon adsorbents for heavy metal recovery that is followed by upcycling of the spent adsorbents *via* H_2O_2 oxidation to catalysts (SDG12) that are effective in a [BMIM]Cl ionic liquid reaction phase for the conversion of C5 carbohydrates into furoic acid as food additives, flavors or monomers (SDG2) and C6 carbohydrates into 5-hydroxymethylfurfural as a platform chemical (SDG7).

1. Introduction

Biomass is a versatile sustainable resource that can be used to produce platform chemicals from energy crops,[1] biofuels from agricultural wastes,[2] functional biocarbons from plant-derived, animal-derived or municipal solid wastes[3] or lignin-based adsorbents from paper industry black liquors.[4] Among the many products derived from biomass, carbonaceous materials known as biocarbons and biochars have gained popularity for use in catalysis, energy and environmental applications.[5] However, with the growth of industrialization in numerous countries, heavy metal contamination due to industrial activities is becoming one of the focal points for material recycling.[6,7] Although nickel is one of the most common heavy metals used in industry (*e.g.* electrical appliances, manufacturing, batteries, and leather tanning),[8] it has severe effects on human health.[9] Compared with other methods such as coagulation,[7] ion exchange,[10] and membrane separation,[11] adsorption methods are energy efficient and economic, and useful for the removal of Ni^{2+} from wastewater.[12] However, existing papers give limited information on the separation of Ni^{2+} by carbon adsorbents compared with studies on other heavy metals (*e.g.* chromium, cadmium or mercury).[9] Most hydrothermal carbonaceous materials prepared from renewable biomass resources require

[a]*Agro-Environmental Protection Institute, Ministry of Agriculture and Rural Affairs, No. 31 Fukang Road, Nankai District, Tianjin 300191, China. E-mail: haixin_g@126.com*

[b]*Graduate School of Environmental Studies, Tohoku University, Aramaki Aza Aoba 468-1, Aoba, Sendai 980-8572, Japan. E-mail: richard.smith.c6@tohoku.ac.jp*

[c]*Department of Industrial System Engineering, Material and Biological Engineering Course, National Institute of Technology (KOSEN), Hachinohe College, 16-1 Uwanotai, Tamonoki-Aza, Hachinohe, 039-1192, Japan*

† Electronic supplementary information (ESI) available. See DOI: https://doi.org/10.1039/d3su00004d

high-temperature carbonization and activation for the preparation of activated carbons (ACs) for wastewater treatment.[6,13] However, renewable functionalized biocarbons (*e.g.* COOH, OH, and amino groups) prepared by the same methods may cause considerable pollution in their processing steps including regeneration of carbons produced by hydrothermal methods.[14,15] Traditionally, inorganic acids (*e.g.* hydrochloric acid) or organic acids (*e.g.* oxalic acid and citric acid) have been used to desorb and regenerate biocarbon adsorbents,[5] all of which lead to considerable environmental pollution. Therefore, recovering these metals directly from the spent adsorbent solids creates much liquid wastes, and hence, sustainability dictates that the spent materials be recycled in a different way, which is denoted as upcycling in this work, since the chemical process step of catalysis occurs upstream rather than downstream as in the final waste treatment step. Upcycling has been reported for the production of copper nanoparticles from acid mine drainage,[16] development of chitosan-based aerogel adsorbents from soot particles,[17] synthesis of hydrogel ion exchange media from waste plastics[18] and simultaneous H_2 fuel production and CO_2 capture from polyethylene terephthalate (PET) wastes.[19] In this study, upcycling of bifunctional catalysts from spent heavy metal functional biocarbon adsorbents for platform chemical production is demonstrated.

Hydrothermal carbonization as well as wet torrefaction has been used to produce functional carbon materials from renewable carbohydrates such as fructose, glucose, cellulose and raw biomass feedstocks.[20,21] Hydrothermal carbonization involves hydrolysis, dehydration, and decarboxylation reactions, which result in carbon materials with oxygen-containing functional groups (–COOH and –OH).[22] Functionalized hydrothermal carbonaceous materials are efficient for the conversion of C5/C6 carbohydrates into chemicals, and they can be designed to contain Brønsted acid sites ($–SO_3H$) depending on the additives.[23,24]

Selective dehydration and oxidation of renewable carbohydrates to acids are some of the most important chemical transformation steps in biomass processing.[25] Several products that can be obtained *via* the oxidation of furfural and 5-hydroxymethylfurfural are furoic acid,[1] 2,5-furandicarboxylic acid[26] and succinic acid,[25] which have application in cosmetic, polymer, and pharmaceutical industries. Furoic acid is widely used as a flavoring and preservative agent, and 2,5-furandicarboxylic acid is an intermediate monomer in the synthesis of polyethylene furoate to replace petrochemical-based monomers.[1,26] In general, the selective oxidation of furfural and 5-HMF requires the presence of noble metal-supported catalysts.[26] Indeed, the direct conversion of C5/C6 carbohydrates into furoic acid using an acid-oxidation catalyst is still a challenge. N-heterocyclic carbene-based materials have been found to be active in the selective oxidation of various furan-based aldehydes.[27] In a previous study, N-functional biocarbons were synthesized by the hydrothermal carbonization of biomass and were shown to effectively adsorb levulinic acid and 5-hydroxymethylfurfural.[24]

In this study, functional biocarbons were prepared by the hydrothermal-ammonia carbonization of cellulose using ammonia-water solutions (Fig. 1, step 1). In general, the adsorption performance capacity of a solid for a metal increases with the increase in solution basicity. Alternatively, $–SO_3H$ groups in a carbonaceous material can be expected to lower the adsorption capacity for a metal. To overcome this limitation, the proposed biocarbons developed in this work introduce Brønsted acid precursor sites into the biocarbons that are converted into Brønsted acid sites in the upcycling process. To avoid sulfonation methods that can generate toxic gases, L-cysteine with its thiol group was used as a precursor to $–SO_3H$ and was introduced into the biocarbon *via* a mechanochemical step (Fig. 1, step 2) and further used after metal adsorption (heavy metal recovery) as a Brønsted acid catalyst for C6 carbohydrate hydrolysis-dehydration (*e.g.* fructose into 5-HMF, cellulose hydrolysis dehydration) and as a hydrolysis–oxidation catalyst in the cascade conversion of C5 carbohydrates into furoic acid. The adsorptive performance of functional biocarbons for removing Ni^{2+} from water (Fig. 1, step 3) and the catalytic activity of Ni-containing functional carbon materials for converting C5/C6 carbohydrates into platform chemicals and biofuels (Fig. 1, step 4) were assessed to demonstrate material upcycling of spent functional biocarbon adsorbents.

2. Materials and experimental

2.1. Materials

Microcrystalline cellulose (particle size = 51 μm, bulk density at 25 °C, 0.6 g mL^{-1}), 1-butyl-3-methylimidazolium chloride ([BMIM]Cl) and 5-hydroxymethylfurfural (99%) were obtained

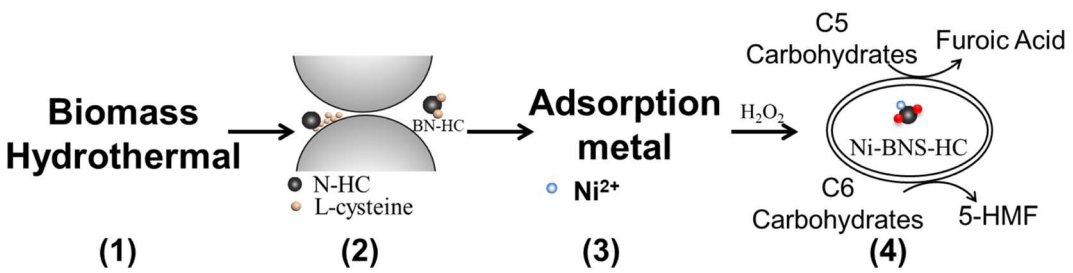

Fig. 1 Four steps producing platform chemicals and biofuels *via* upcycling of carbonaceous solids: (1) hydrothermal carbonization (HC) of cellulose in ammonia-water solutions to form N-HC, (2) ball-milling of N-HC with L-cysteine to form BN-HC, (3) adsorption of Ni^{2+} as a nickel recovery step from wastewater, and (4) upcycling of spent adsorbents *via* H_2O_2 to form Ni-BNS-HC for oxidation–dehydration catalysts.

from Sigma-Aldrich (Japan). The chemicals D-xylose, D-fructose, D-glucose (98%), levulinic acid (99%), L-cysteine, furfuryl alcohol (98%), furfural (98%), ammonia solution (25.0%), ethanol (99.5%), copper(II) nitrate trihydrate (99.9%), zinc nitrate hexahydrate (99%), nickel(II) nitrate hexahydrate (98%), cobalt(II) nitrate hexahydrate (98%), sodium hydroxide (97%), sodium carbonate (>99%), standards in nitric acid, nickel standard solution (Ni 1000), zinc standard solution (Zn 1000), copper standard solution (Cu 1000) and cobalt standard solution (Co 1000), 1.0% w/v phenolphthalein ethanol (90) solution, sodium hydroxide solution (0.1 mol L^{-1}), sodium bicarbonate (>99.5%), standard hydrochloric acid solution (0.1 mol L^{-1}) and hydrochloric acid were purchased from Wako Pure Chemical Industries, Ltd (Osaka). All chemicals were used as received without further purification.

2.2. Preparation of biocarbons

Many works have studied hydrothermal carbonization of cellulose at around 200 °C using reaction times of 4 to 24 h.[28] By prolonging the reaction time, the amount of hydrolyzed products, the O/C ratio and the H/C ratio tend to decrease.[28] In this work, amino-functional carbons were prepared by hydrothermal-ammonia carbonization of cellulose (16 g) and ammonia solution (5%, 50 mL) in a 200 mL stainless autoclave *via* heating the materials at 200 °C for 8 h. The resulting crude black carbon was washed repeatedly with ethanol and water, oven-dried at 60 °C under vacuum conditions for one day and denoted as N-HC. Blank carbonized solids were prepared without additives of the ammonia solution under the same conditions as those used in preparing N-HC, and are denoted as HC.

2.3. Preparation of amino-Brønsted acid precursor functional biocarbon adsorbents

Generally, amino-Brønsted acid precursor functional biocarbons were synthesized in a ball mill (Retsch MM 500), in which 100 g of the ball (5 mm in diameter) were mixed with 1.0 g of freshly prepared biocarbon (HC or N-HC) and 2.0 g of L-cysteine at 600 rpm for 4 h. The resulting solids were washed with water, oven-dried at 60 °C under vacuum conditions for one day and denoted as B-HC and BN-HC, respectively.

2.4. Adsorption experiments

The procedure used in the adsorption experiments is similar to that reported previously.[14] Briefly, a solution of $Ni(NO_3)_2$ in water (20 mL, 50 mM, pH 6.6) and 0.05 g of as-prepared carbon were stirred at room temperature (25 °C) for a given period of time and then the solution was filtered to separate the solid adsorbent from the liquid. The adsorbent was oven-dried at 60 °C under vacuum conditions for 12 h and denoted as Ni-B-HC or Ni-BN-HC depending on the starting material. The amount of metal ions in the liquid solution over time was analyzed by ICP-AES (Thermo Fisher, iCAP6500). Quantitative analysis of the adsorbent capacity of the as-prepared functional carbons for the removal of Ni^{2+} ions was performed according to eqn (1):

$$Q_e = \frac{(C_i - C_f) \times V}{m} \quad (1)$$

where Q_e is the amount of Ni^{2+} ions adsorbed onto a unit amount of functional carbon (mg g^{-1}), and C_i and C_f are the concentrations (mg L^{-1}) of Ni^{2+} ions before adsorption and after equilibrium, respectively. In eqn (1), V is the volume of the solution and m is the mass of adsorbent (g). Under saturation conditions, C_f is defined as C_s.

Saturated adsorption capacity (Q_s) was correlated with the Langmuir and Freundlich models as given by eqn (2) and (3), respectively:

$$Q_s = \frac{Q_m K_L C_s}{1 + K_L C_s} \quad (2)$$

$$Q_s = K_F C_s^{1/n} \quad (3)$$

where K_L is the Langmuir constant, Q_m is the maximum adsorption capacity, K_F is the Freundlich constant and n is the adsorption intensity. The pH value of the solution was analysed using a LAQUA pH meter F-71 (Horiba, Japan).

2.5. Preparation of Brønsted acid site amino-functional biocarbons

Functional biocarbons after Ni^{2+} adsorption (Ni-B-HC and Ni-BN-HC) and fresh biocarbons (B-HC and BN-HC) were used as precursors for the preparation of Brønsted acid site amino-functional biocarbon catalysts. After the adsorption of the metal, H_2O_2 was used to oxidize the SH groups into $-SO_3H$. Generally, the as-prepared adsorbent (0.3 g) was immersed in H_2O_2 (15 mL solution) with methanol (15 mL) and stirred magnetically at room temperature for 24 h. After 24 h, the solids were washed with water and oven-dried at 60 °C under vacuum conditions for one day and denoted as BS-HC, BNS-HC, Ni-BS-HC and Ni-BNS-HC.

2.6. Reaction experiments and products analyses

Generally, 0.05 g of biocarbon, 2 g of ionic liquid as a reaction solvent and a given amount of substrate (0.1 g) were loaded into a stainless-steel autoclave with a Teflon liner (15 mL) and the stainless-steel autoclave was placed into a preheated oil bath with magnetic stirring. After the reaction was terminated, the reaction solution was collected with repeated washings of the reaction tube of distilled water and reaction products were analyzed by high-performance liquid chromatography (HPLC). HPLC analysis was performed using a JASCO system equipped with a refractive index detector RI-4030 and a UV-Vis detector with a SH1011 column (Shodex) containing 0.5 mM sulfuric acid as the mobile phase (0.5 mL min^{-1}) at 50 °C. Substrate conversion and product yields were calculated using eqn (4) and (5):

$$\text{Conversion} \quad (\%) = \left(1 - \frac{\text{moles of substrate, final}}{\text{moles of substrate, initial}}\right) \times 100 \ (\%) \quad (4)$$

$$\text{Yield } (\%) = \frac{\text{moles of product, final}}{\text{moles of substrate, initial}} \times 100\ (\%) \quad (5)$$

2.7. Characterization

The as-prepared carbon materials were characterized using an X-ray diffractometer (XRD, MiniFlex 600, Rigaku) equipped with a monochromatic light source, Cu K_α radiation, and the samples were scanned in the 2θ range from 10° to 80°. Raman spectra analysis was conducted using a micro-Raman spectrometer (HORIB Scientific LabRAM HR Evolution). FT-IR measurements were performed using a Thermo Scientific Nicolet iS20 spectrometer in the range of 400–4000 cm^{-1} after mixing the carbon sample with a KBr powder. Surface elemental valence analysis (C, O, N, and S) was performed using a X-ray photoelectron spectrometer (XPS, Axis-Ultra, Shimadzu) with a pass energy of 20 eV. The Vision 2 Processing software (Kratos Analytical) was used for curve-fitting the XPS results. The specific surface area of the as-prepared samples was determined by the measurement of nitrogen absorption–desorption isotherms (BELSORP-mini, BEL Inc., Japan). The morphology of the as-prepared carbon was observed by acquiring SEM images using a FE-SEM (HITACHI-4800) operating at 15.0 kV × 500–2000. SEM-EDX elemental mappings were obtained using a Horiba/EX-420. The SEM samples were coated with gold by sputtering. The surface area and pore diameters (D_p) of the samples were estimated by the BET method using the BELMaster™ software. The amount of functional groups in the as-prepared samples was measured by the Boehm method.[29]

2.8. Basis for the density functional theory calculations

Density functional theory (DFT) calculations for Ni^{2+} with carbon complexes were calculated with the unrestricted M06 level of theory.[30] The basis sets for C, N, O, and H atoms were used 6-31G(d,p). The SDD basis set for the Ni atom was used with Stuttgart/Dresden effective core potential. The solvation effect in water was applied as the SMD solvation model.[31] The geometry optimization calculation was performed for the Ni–carbon complex and monomers, followed by frequency calculations to apply thermochemical correction at 298 K and 1 atm. The conformation energies for the Ni–carbon complex were calculated as the energy difference between the Ni–carbon complex and its monomers. All DFT calculations were performed using Gaussian 16 Rev. C01.[32]

3. Results and discussion

3.1. Characterization

XRD measurements of the as-prepared functional biocarbons (Fig. S1†) showed that there were no large differences in the patterns between HC and N-HC materials. The XRD patterns of the biocarbons exhibited two peaks at around 23° and 44°, corresponding to (002) and (100) that could be attributed to the planes of amorphous carbons.[33] The surface areas and pore diameters of the as-prepared biocarbons were determined by N_2 adsorption–desorption (Table S1†). The biocarbons had low surface area (<5 $m^2\ g^{-1}$) with a pore diameter of 17 to 25 nm. The morphologies of hydrothermal biocarbons (HC or N-HC) and mechanochemical (ball-milling) treatment biocarbons (B-HC and BN-HC) were bulk-like and flake-like with no apparent holes (Fig. S2†); after adsorption and oxidation treatment, biocarbons (Ni-BNS-HC) had a rough surface (Fig. S2e†). As shown in the SEM images, B-HC and BN-HC had different particle sizes compared with their blank counterparts, HC and N-HC, respectively (Fig. S2 and S3†). The SEM-EDX mapping of HC and B-HC materials showed that after ball-milling treatment, S atoms were distributed homogeneously on the carbon solids (Fig. S4†). While the ash content of raw cellulose is less than 0.5%,[34] that of hydrothermal carbon HC and N-HC increased to 1.3% and 1.4%, respectively. The elemental content (carbon, oxygen, nitrogen and sulfur) of the as-prepared biocarbons was determined by XPS (Table S1†). Compared with the blank material (HC), a new peak for N-HC appeared at around 400 eV that could be attributed to amino groups, which confirmed nitrogen ions being incorporated into the biocarbon structure. A new peak for B-HC appeared at around 400 eV that could be attributed to additional amino groups (Fig. S5†). Moreover, considering analyses of HC and N-HC along with new peaks appearing at around 165 eV for B-HC and BN-HC that could be attributed to sulfur groups,[35] it can be concluded that there were interactions between hydrothermal carbons (HC or N-HC) and L-cysteine after the mechanochemical (ball-milling) process treatment. It is probable that some –SH oxidation occurred during the ball-milling process under air atmosphere conditions.

The C 1s spectra of the biocarbons can be deconvoluted into four peaks ascribed to C–C/C=C (~284.6 eV), C–O (~286.3 eV), C=O (~287.8 eV) and O–C=O (~289.1 eV) (Fig. S6†).[35] The O 1s spectra of HC exhibited one peak ascribed to C–OH (532.3 eV), whereas the N-HC, B-HC and BN-HC samples exhibited additional peaks assigned to O–N (~530.4 eV) and O–C=O (~534.1 eV) (Fig. S7†), which shows that the as-prepared biocarbon samples synthesized in this work had abundant oxygen-containing groups (C–OH and COOH) and amino groups on their surface. The binding energy of O 1s and C 1s for B-HC (532.6 eV and 285.6 eV) and BN-HC (532.1 eV and 285.1 eV) samples slightly shifted as compared to that of HC (532.1 eV and 285.2 eV) and N-HC (531.8 eV and 284.8 eV), which implies that mechanochemistry treatment caused surface changes in the HC and N-BC samples. The quantification of the functional groups of the biocarbons (Table S1†) showed that BN-HC had the highest nitrogen content compared with the other samples (HC, N-HC and B-HC). In Fig. S8,† two major peaks were observed after ball-milling treatment of samples B-HC and BN-HC at around 166 eV and 161 eV that correspond to sulfite and –SH;[36] however, it is likely that oxidation of some of the thiol groups occurred during the ball-milling process under air atmosphere conditions.

3.2. Adsorption of metal ions

The adsorption of Ni^{2+} ions onto the functional biocarbons was studied (Fig. 2a), where it was found that the amount of metals

removed from the solution increased with time at constant temperature for all samples. Generally, the rate of Ni^{2+} removal onto amino-functionalized biocarbons (N-HC and BN-HC) was higher than that of the non-aminated sample (HC), which suggests that the introduction of amino-groups into the biocarbon increases adsorption performance (rate and capacity). Compared with B-HC, HC was more effective for the removal of Ni^{2+} ions from the aqueous solution (Fig. 2a), which is possibly due to HC having high –COOH content than that of B-HC (Table S1†). An adsorption capacity of 115 mg g^{-1} (initial pH = 6.6) was obtained at about 50 h for BN-HC samples. The maximum adsorption capacities Q_m of biocarbons and other adsorbents such as glycine-functionalized silica,[9] polyvinylpyrrolidone-coated magnetite nanoparticles[37] and biomass-based activated carbons[38] are 9.7140.8 mg g^{-1} for Ni^{2+}, where it can be seen that the as-prepared biocarbons had high capacities for separating Ni^{2+} from water and they are probably more efficient than the other proposed adsorbents shown.

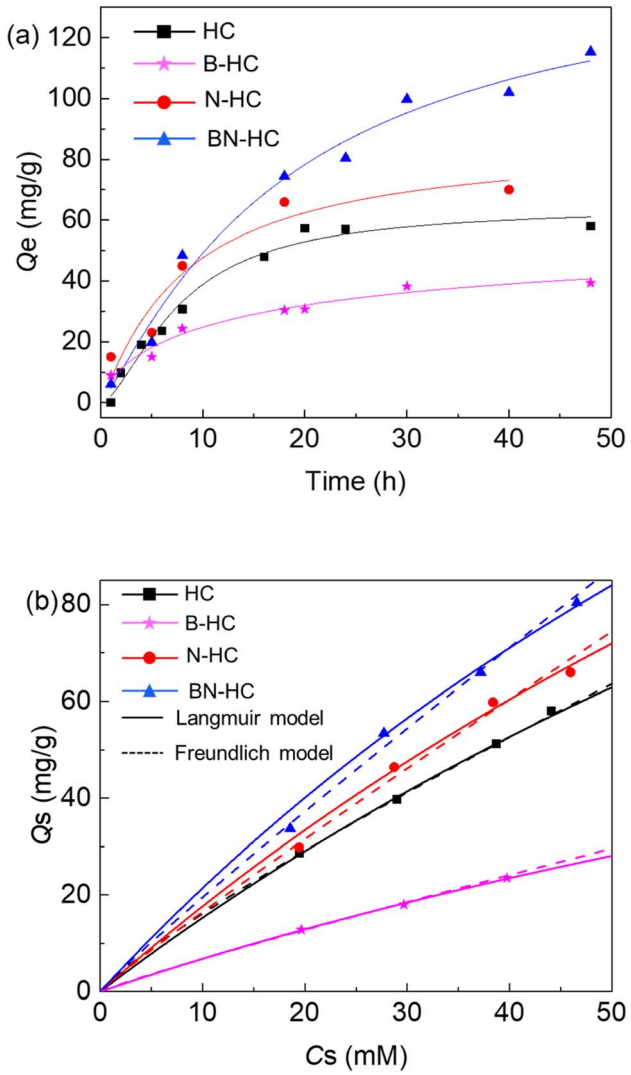

Fig. 2 Adsorption of Ni^{2+} onto HC, B-HC, N-HC, and BN-HC: (a) adsorption kinetics fitted with the Langmuir model and (b) adsorption isotherms fitted with the Langmuir model (solid line) and Freundlich model (dashed line). Conditions of the adsorption kinetic study (a): 20 mL of 50 mM of Ni^{2+}, initial pH 6.6, 0.05 g of adsorbent, 20 °C; conditions for the adsorption isotherms study (b): 20 mL of Ni^{2+} solution, 0.05 g of adsorbent, 20 °C, after 20 h.

In the adsorption experiments with the biocarbons, the pH of the aqueous liquid phase decreased from 6.6 to 5.4 as adsorption progressed, which could be attributed to ion exchange occurring between H^+ at the oxygenated groups (*e.g.* COOH and OH) of the biocarbons and the release of the Ni^{2+} ion.[38] The effect of initial pH on Ni^{2+} adsorption by BN-HC is shown in Fig. S9a.† The adsorption capacity of Ni^{2+} ions increased from 5.1 mg g^{-1} to nearly 100 mg g^{-1} when the initial pH changed from 4 to 6.68. A further increase in the initial pH resulted in a decrease in the adsorption capacity of BN-NC for Ni^{2+}, which may be due to the number of binding sites available in the adsorbent, which become protonated at low pH resulting in low binding of cations. Moreover, the adsorption of Ni^{2+} ions was not only due to oxygen-containing functional groups (–COOH, –OH), but also due to amino-functional groups that increase the adsorption capacity due to combinations of hydroxyl and amino groups.[14,15]

Table 1 and Fig. S8† show the conformation energy and optimized structures for Ni-carbon complexes. The Ni-carbon complexes with two carboxylic acid groups (Fig. S2a†) show a conformation energy of −514.7 kJ mol^{-1}, with the carboxylic group having strong adsorption due to ion exchange adsorption mechanism. For the case of combinations of carboxylic anions with hydroxy groups, and carboxylic anions with amino groups, the conformation energies for the complexes were −447.2 kJ mol^{-1} and −433.2 kJ mol^{-1}, respectively (Table 1). The low conformation energy with a carboxylic group indicates that the number of carboxylic groups has an important role in the adsorption mechanism. The optimized structures of the complex with hydroxy and amino groups had complexes with bifurcated coordination bonds from Ni^{2+} ions to hydroxy and amino groups (Fig. S8d and f†). The combination effect among functional groups can form bifurcated coordination structures, which would increase the adsorption capacity, but not necessarily increase the adsorption efficiency, because ligand formation with cysteine is a function of pH[39] and is favored with

Table 1 Conformation energies for the Ni–carbon complex, and single-point energies of Ni–carbon complexes and monomers. Conformation and single-point energies were applied thermochemical corrections by frequency calculations. Single-point energy for Ni^{2+} is −170.45008 au

Functional groups		Energies		
Group 1	Group 2	Complex (au)	Functionalized carbon (au)	Conformation (kJ mol^{-1})
$-NH_2$	$-NH_2$	−820.15276	−649.54606	−411.2
$-NH_2$	$-COO^-$	−952.87213	−782.25706	−433.2
$-NH_2$	–OH	−840.03239	−669.43006	−399.7
$-COO^-$	$-COO^-$	−1085.6089	−914.96276	−514.7
$-COO^-$	–OH	−972.75441	−802.13400	−447.2
–OH	–OH	−859.88225	−689.30599	−331.3

cysteine at high pH according to the studies with small peptides.[40]

The effect of functional groups on the equilibrium amount of Ni^{2+} adsorbed onto the biocarbon adsorbent (HC, B-HC, N-HC and BN-HC) was evaluated by varying the initial Ni^{2+} ion solution concentration. Langmuir and Freundlich adsorption isothermal curves (Fig. 2b) and the calculated parameters are given in Table S2.† The adsorption of Ni^{2+} followed the Freundlich isotherm with coefficients greater than 0.98 for all systems, while lower correlation coefficients (R^2 = 0.87–0.93) were observed for the Langmuir model (Table S2†), which could be attributed to the high range of equilibrium concentrations, high adsorption capacities of the solids and the inherent assumptions in each model. The Freundlich model described the adsorption behavior better than the Langmuir model, implying that adsorption of Ni^{2+} onto the biocarbon adsorbents has heterogeneous characteristics due to site interactions including chemical adsorption. The maximum capacities of HC, B-HC, N-HC and BN-HC for Ni^{2+} were calculated to be 285.7 mg g^{-1}, 130 mg g^{-1}, 312.5 mg g^{-1}, and 313.5 mg g^{-1}, respectively. The analysis of the residuals from the Langmuir and Freundlich models with the F-test (Table S3†) showed that the two-tailed probabilities were greater than 0.05 for the HC and N-HC systems and less than 0.05 for the B-HC and BN-HC systems. Therefore, for the HC and N-HC systems, either Langmuir or Freundlich models provide similar correlation of the data (Fig. 2, Tables S2 and S3†). However, for the B-HC and BN-HC systems, residuals from the Freundlich model are statistically distinguishable from those of the Langmuir model and the Freundlich model provides better correlation of the data than the Langmuir model (Fig. 2, Tables S2 and S3†). To better mimic real environmental conditions, the adsorption of different metals onto the biocarbons (HC) was studied (Fig. S9b†), which showed that Ni^{2+} and Cu^{2+} had higher adsorption onto HC than other metals.

3.3. Upcycling of spent adsorbents to catalysts

To study upcycling of the Ni^{2+}-containing spent adsorbent, H_2O_2 was used to oxidize thiol (–SH) groups of the spent adsorbent into Brønsted acid (–SO_3H) sites. XPS analysis was used to confirm the elemental content in Ni-BNS-HC. Compared with the fresh adsorbent BN-HC, the percentage of carbon in Ni-BN-HC decreased to 30.7%, while the percentage of oxygen increased to 59.7% (Table S1†). After the oxidation of Ni-BNS-HC samples with the H_2O_2 solution, the S 2p spectra of Ni-BNS-HC exhibited new peaks of sulfate at ~169.7 eV and ~168.4 eV, as reported in the literature (Fig. S10†),[36] which demonstrates that thiol sites on the functional carbon were oxidized into Brønsted acid sites. Functional groups such as OH (at around 3400 cm^{-1}), –COOH (at around 1680 cm^{-1}) and sulfonate groups (at around 1010 cm^{-1} and 1160 cm^{-1}) were confirmed to exist and to be stable on the adsorbent biocarbon after the adsorption of Ni and oxidation treatment according to FT-IR analyses (Fig. S11a†). The peak at around 676 cm^{-1} is assigned to the Ni–O bending vibrations[41] that may affect the catalytic performance. The Raman spectra of biochar (N-HC, BN-HC and Ni-BNS-HC) exhibited two characteristic peaks of carbon, namely, D band from sp^3 disordered carbon (~1360 cm^{-1}) and G band resulting from sp^2 graphic nature carbon (~1590 cm^{-1}). The I_D/I_G values of BNS-HC (2.8) were lower than those of Ni-BNS-HC (4.7) (Fig. S11b†), which infers that after oxidation, the Ni-BNS-HC material had the lower degree of graphitization. Py-FTIR measurements (Fig. S11c†) showed that Ni-BNS-HC had both Lewis acid (L) sites (59.2 μmol g^{-1}) and Brønsted acid (B) sites (3.8 μmol g^{-1}). Reactions with spent adsorbents and C5/C6 carbohydrate substrates were performed to assess the biocarbon (oxidized spent adsorbent) catalytic activity. Xylose was used to determine initial reaction conditions (Table 2) and to demonstrate the proof of concept of upcycling. When only Ni^{2+} ions existed in the solution in the reaction system, no furfural and furoic acid (2-FAD) products were formed (entry 1, Table 2). However, when reactions were performed in the presence of biocarbons (BS-HC and BNS-HC), conversion (>70%), furfural yields (>19%) and 2-FAD yields (>23%) all increased due to functional groups on the biocarbons. Brønsted acid sites (–SO_3H) on the biocarbons are highly active for promoting xylose dehydration into furfural, while nitrogen-containing group sites (–NH) are highly active for promoting the oxidation of furfural into furoic acid.[1] When Ni-based biocarbons were used (Ni-BS-HC and Ni-BNS-HC), furoic acid yields increased (39.8–46.2%) over the functional carbons BS-HC and BNS-HC, respectively (entries 2–5, Table 2), which is evidence that Ni in the biocarbon enhances the conversion of furfural into 2-FAD. Moreover, Ni acts as a Lewis acid site to promote the conversion of xylose into furfural and xylose isomerization into isomer intermediates (*e.g.* xylulose).[42] At the same time, Brønsted acid sites of the biocarbons also promote the conversion of isomer intermediates into furfural. In all reaction systems, xylose conversions were always higher than the total yield of furfural and 2-FAD, which can be explained by unavoidable furfural decomposition or polymerization in the presence of acid catalysts.[26] However, fair yields of furfural and 2-FAD could be obtained with the as-prepared and spent adsorbent biocarbons as compared with literature results,[42,43] thus demonstrating upcycling of the biocarbons. Carbon balances for the conversion of xylose with Ni-BS-HC or Ni-BNS-HC at 150 °C after 4 h reaction time (Fig. S12†) were

Table 2 Conversion of C5 carbohydrate substrates into furfural and furoic acid (2-FAD) with catalytic materials. Reaction conditions: 0.1 g of xylose, 0.05 g of catalyst, 3 g of [BMIM]Cl, at 150 °C after 4 h reaction time

			Yield (%)	
Entry	Material	Conv. (%)	Furfural	2-FAD
1[a]	Ni^{2+} ion	>60	—	—
2	BS-HC	78.2	40.6	32.3
3	Ni-BS-HC	81.4	28.5	39.8
4	BNS-HC	71.1	19.5	23.7
5	Ni-BNS-HC	74.4	24.7	46.2

[a] 0.5 mL of nickel standard solution (Ni 1000) as $Ni(NO_3)_2$.

from 75% to 81%. For the case of Ni-BS-HC or Ni-BNS-HC using xylose as the substrate, nearly 9.7% or 2.3% yields of humins were obtained.

The Ni-BNS-HC biocarbons were investigated as catalysts for the conversion of C6 carbohydrates (Table 3). Ni-BNS-HC was active for promoting the dehydration of fructose into 5-HMF (Table 3), although yields of 5-HMF from glucose and cellulose were lower than those obtained from fructose substrate (entries 2–7, Table 3). The Ni-BNS-HC biocarbon could promote dehydration of fructose and also isomerization of glucose to fructose (entry 2, Table 3). Increasing the reaction temperature from 160 °C to 180 °C led to a decrease in total reducing sugars and 5-HMF yield but a small increase in the LA yield (entries 3 and 5, Table 3). The catalytic reaction of C6 carbohydrates with Ni-BNS-HC also led to levulinic acid (LA) formation (Table 3).

3.4. Recycle of catalysts

The recycle of Ni-BNS-HC biocarbons was studied for the fructose substrate. Recycle experiments were conducted at 120 °C for 1.5 h reaction time. After each reaction run, the Ni-BNS-HC biocarbon was separated from the reaction solution, washed with water and dried at 60 °C for 24 h. As shown in Fig. S13a,† the Ni-BNS-HC biocarbon remained active after four runs with about 5% loss in catalytic activity per run despite mass changes of catalysts that occur during washing and drying steps. The decrease in the 5-HMF yields along with the number of recycles could be attributed to the adsorption of humin precursors onto the catalyst that cause particle aggregation along with the loss of active sites and mass loss that occurs in the filtration–washing steps. The loss of nickel metal in each step of the recycle procedure was examined by ICP, in which about 4.4% of nickel metal was concluded to leach into the reaction solution. At least two methods are available to prevent nickel from entering the environment. First, by applying recycle treatment to a fresh catalyst, the amount of nickel lost due to catalyst attrition can be lowered. Second, by applying fresh adsorbents to spent reaction solutions, it is possible to recover leached Ni and prevent it from entering the environment. The FT-IR results of the recycled catalyst showed no noticeable changes in catalyst structure with use, suggesting that S is stably bound (Fig. S13b†). Furthermore, recycle results for the Ni-BNS-HC biocarbon confirmed that the Brønsted acid active sites were stable under reaction conditions and that multiple uses of the upcycled spent adsorbent were feasible.

Table 3 Conversion of C6 carbohydrates with Ni-BNS-HC (TRS: total reducing sugars, LA: levulinic acid). Reaction conditions: 0.1 g of substrates (fructose or glucose), 0.05 g of catalyst and 2 g of [BMIM]Cl; 0.1 g of cellulose, 0.05 g of catalyst, 2 g of [BMIM]Cl and 20 μL of water

					Product yield (%)		
Entry	Substrate	T (°C)	Time (h)	Conv. (%)	TRS	HMF	LA
1	Fructose	160	4	100	—	71	2.4
2	Glucose	160	4	100	17.0[a]	24	—
3	Cellulose	160	4	—	46.5	4.7	—
4	Cellulose	180	2	—	9.9	1.5	<5
5	Cellulose	180	4	—	18.5	7.7	<5
6	Cellulose	180	6	—	6.1	11.1	<5
7	Cellulose	180	8	—	5.3	9.7	<5

[a] Yield of fructose.

4. Conclusions

Aminated functional biocarbons suitable for heavy metal recovery were synthesized by hydrothermal-ammonia carbonization and a thiol mechanochemical mix-milling method. The synthesized biocarbons exhibited remarkable adsorption capacity for Ni^{2+} ions and spent adsorbents could be upcycled as catalysts after oxidation to promote the conversion of furfural and 5-hydroxymethylfurfural into furoic acid, while other C5/C6 carbohydrates could be converted into corresponding products in favorable yields. The developed biocarbons with Brønsted acid sites show promise in material upcycling schemes for removing spent heavy metals from wastestreams *via* adsorption and subsequent use as catalysts for dehydration–oxidation of C5/C6 carbohydrate substrates.

Author contributions

Yuto Inoue: methodology, investigation, data curation. Yukiya Isoda: investigation, data curation. Haixin Guo: methodology, writing-original draft-review & editing, project administration, funding acquisition. Tetsuo Honma; data curation; writing-review & editing. Richard Lee Smith Jr: methodology, writing-review & editing, project administration, funding acquisition. The experimental research was performed at Tohoku University. All authors discussed the results and contributed to the manuscript (*e.g.* Writing – original draft, writing – review & editing).

Conflicts of interest

There are no conflicts to declare.

Acknowledgements

The authors are grateful for Basic Frontier Project of Agro-Environmental Protection Institute, Ministry of Agriculture and Rural Affairs of China (2022-jcqyrw-ghx), Elite Youth program of the Chinese Academy of Agricultural Sciences (to Haixin Guo) and from the Materials Processing Science project ("Materealize") of the Ministry of Education, Culture, Sports, Science and Technology (MEXT) (Grant Number JPMXP0219192801).

References

1 N. K. Gupta, A. Fukuoka and K. Nakajima, Metal-free and selective oxidation of furfural to furoic acid with an N-heterocyclic carbene catalyst, *ACS Sustain. Chem. Eng.*, 2018, **6**(3), 3434–3442.

2 Y. Nie, Q. Hou, H. Qian, X. Bai, T. Xia, R. Lai, G. Yu, M. L. Ur Rehman and M. Ju, Synthesis of mesoporous sulfonated carbon from chicken bones to boost rapid conversion of 5-hydroxymethylfurfural and carbohydrates to 5-ethoxymethylfurfural, *Renewable Energy*, 2022, **192**, 279–288.
3 Y. Shen, Biomass-derived porous carbons for sorption of Volatile organic compounds (VOCs), *Fuel*, 2022, 126801.
4 H. A. Hamad, S. E. AbdElhafez, M. M. Elsenety, M. K. Sorour, N. K. Amin, O. Abdelwahab and E. S. Z. El-Ashtoukhy, Fabrication and characterization of functionalized lignin-based adsorbent prepared from black liquor in the paper industry for superior removal of toxic dye, *Fuel*, 2022, **323**, 124288.
5 M. M. Titirici, R. J. White, N. Brun, V. L. Budarin, D. S. Su, F. Del Monte, J. H. Clark and M. J. MacLachlan, Sustainable carbon materials, *Chem. Soc. Rev.*, 2015, **44**(1), 250–290.
6 J. Kong, R. Gu, J. Yuan, W. Liu, J. Wu, Z. Fei and Q. Yue, Adsorption behavior of Ni(II) onto activated carbons from hide waste and high-pressure steaming hide waste, *Ecotoxicol. Environ. Saf.*, 2018, **156**, 294–300.
7 G. Peng, S. Deng, F. Liu, C. Qi, L. Tao, T. Li and G. Yu, Calcined electroplating sludge as a novel bifunctional material for removing Ni(II)-citrate in electroplating wastewater, *J. Cleaner Prod.*, 2020, **262**, 121416.
8 J. Piątek, T. M. Budnyak, S. Monti, G. Barcaro, R. Gueret, E. S. Grape, A. Jaworski, A. K. Inge, B. V. M. Rodrigues and A. Slabon, Toward sustainable Li-Ion battery recycling: green Metal-Organic Framework as a molecular sieve for the selective separation of cobalt and nickel, *ACS Sustainable Chem. Eng.*, 2021, **9**(29), 9770–9778.
9 J. Piatek, C. N. de Bruin-Dickason, A. Jaworski, J. H. Chen, T. Budnyak and A. Slabon, Glycine-functionalized silica as sorbent for cobalt(II) and nickel(II) recovery, *Appl. Surf. Sci.*, 2020, **530**, 12.
10 P. E. Franco, M. T. Veit, C. E. Borba, G. d. C. Gonçalves, M. R. Fagundes-Klen, R. Bergamasco, E. A. da Silva and P. Y. R. Suzaki, Nickel(II) and zinc(II) removal using Amberlite IR-120 resin: Ion exchange equilibrium and kinetics, *Chem. Eng. J.*, 2013, **221**, 426–435.
11 H. Duan, H. Liu, C. Hu, X. Yang and X. Wang, Highly efficient and selective membrane separation of copper from nickel in ammoniacal solution using mixtures of M5640 and BESO as membrane carriers, *RSC Adv.*, 2020, **10**(32), 18860–18867.
12 M. Ferri, S. Campisi and A. Gervasini, Nickel and cobalt adsorption on hydroxyapatite: a study for the de-metalation of electronic industrial wastewaters, *Adsorption*, 2019, **25**, 649–660.
13 J. Q. Deng, Y. Q. Liu, S. B. Liu, G. M. Zeng, X. F. Tan, B. Y. Huang, X. J. Tang, S. F. Wang, Q. Hua and Z. L. Yan, Competitive adsorption of Pb(II), Cd(II) and Cu(II) onto chitosan-pyromellitic dianhydride modified biochar, *J. Colloid Interface Sci.*, 2017, **506**, 355–364.
14 Y. Inoue, H. Guo, T. Honma and R. L. Smith, Amino-functional biocarbon with CO_2-responsive property for removing copper(II) ions from aqueous solutions, *Colloids Surf., A*, 2021, **616**, 126304.
15 Q. Q. Guan, K. X. Gao, P. Ning, R. R. Miao and L. He, Value-added utilization of paper sludge: Preparing activated carbon for efficient adsorption of Cr(VI) and further hydrogenation of furfural, *Sci. Total Environ.*, 2020, **741**, 10.
16 R. A. Crane and D. J. Sapsford, Selective formation of copper nanoparticles from acid mine drainage using nanoscale zerovalent iron particles, *J. Hazard. Mater.*, 2018, **347**, 252–265.
17 M. Salzano de Luna and M. Sirignano, Upcycling soot particles into chitosan-based aerogels for water purification from organic pollutants, *J. Hazard. Mater. Lett.*, 2021, **2**, 100019.
18 X. H. Yue, F. S. Zhang, C. C. Zhang and P. Qian, Upcycling of blending waste plastics as zwitterionic hydrogel for simultaneous removal of cationic and anionic heavy metals from aqueous system, *J. Hazard. Mater.*, 2022, **432**, 128746.
19 H. Su, T. Li, S. Wang, L. Zhu and Y. Hu, Low-temperature upcycling of PET waste into high-purity H_2 fuel in a one-pot hydrothermal system with in situ CO_2 capture, *J. Hazard. Mater.*, 2023, **443**, 130120.
20 L. Yan, J. Yu, J. Houston, N. Flores and H. Luo, Biomass derived porous nitrogen doped carbon for electrochemical devices, *Green Energy Environ.*, 2017, **2**(2), 84–99.
21 Y. Wen, Z. Yu, K. Li, H. Guo, Y. Dai and L. Yan, Fabrication of biobased heterogeneous solid Brønsted acid catalysts and their application on the synthesis of liquid biofuel 5-ethoxymethylfurfural from fructose, *Green Energy Environ.*, 2018, **3**(4), 384–391.
22 H. Guo, Y. Hiraga, X. Qi and R. L. Smith Jr, Hydrogen gas-free processes for single-step preparation of transition-metal bifunctional catalysts and one-pot γ-valerolactone synthesis in supercritical CO_2 -ionic liquid systems, *J. Supercrit. Fluids*, 2019, **147**, 263–270.
23 A. Gallifuoco, A new approach to kinetic modeling of biomass hydrothermal carbonization, *ACS Sustain. Chem. Eng.*, 2019, **7**(15), 13073–13080.
24 H. Guo, Y. Hirosaki, X. Qi and R. Lee Smith Jr, Synthesis of ethyl levulinate over amino-sulfonated functional carbon materials, *Renewable Energy*, 2020, **157**, 951–958.
25 W. Zhu, F. Tao, S. Chen, M. Li, Y. Yang and G. Lv, Efficient oxidative transformation of furfural into succinic acid over acidic metal-free graphene oxide, *ACS Sustain. Chem. Eng.*, 2019, **7**(1), 296–305.
26 K. Gupta, R. K. Rai, A. D. Dwivedi and S. K. Singh, Catalytic aerial oxidation of biomass-derived furans to furan carboxylic acids in water over bimetallic nickel-palladium alloy nanoparticles, *ChemCatChem*, 2017, **9**(14), 2760–2767.
27 M. N. Hopkinson, C. Richter, M. Schedler and F. Glorius, An overview of N-heterocyclic carbenes, *Nature*, 2014, **510**(7506), 485–496.
28 N. Paksung, J. Pfersich, P. J. Arauzo, D. Jung and A. Kruse, Structural effects of cellulose on hydrolysis and carbonization behavior during hydrothermal treatment, *ACS Omega*, 2020, **5**(21), 12210–12223.

29 F. Adib, A. Bagreev and T. J. Bandosz, Analysis of the relationship between H_2S removal capacity and surface properties of unimpregnated activated carbons, *Environ. Sci. Technol.*, 2000, **34**(4), 686–692.

30 Y. Zhao and D. G. Truhlar, The M06 suite of density functionals for main group thermochemistry, thermochemical kinetics, noncovalent interactions, excited states, and transition elements: Two new functionals and systematic testing of four M06-class functionals and 12 other functionals, *Theor. Chem. Acc.*, 2008, **120**(1–3), 215–241.

31 A. V. Marenich, C. J. Cramer and D. G. Truhlar, Universal solvation model based on solute electron density and on a continuum model of the solvent defined by the bulk dielectric constant and atomic surface tensions, *J. Phys. Chem. B*, 2009, **113**(18), 6378–6396.

32 M. J. Frisch, G. W. Trucks, H. B. Schlegel, G. E. Scuseria, M. A. Robb, J. R. Cheeseman, G. Scalmani, V. Barone, G. A. Petersson, H. Nakatsuji, X. Li, M. Caricato, A. V. Marenich, J. Bloino, B. G. Janesko, R. Gomperts, B. Mennucci, H. P. Hratchian, J. V. Ortiz, A. F. Izmaylov, J. L. Sonnenberg, D. Williams-Young, F. Ding, F. Lipparini, F. Egidi, J. Goings, B. Peng, A. Petrone, T. Henderson, D. Ranasinghe, V. G. Zakrzewski, J. Gao, N. Rega, G. Zheng, W. Liang, M. Hada, M. Ehara, K. Toyota, R. Fukuda, J. Hasegawa, M. Ishida, T. Nakajima, Y. Honda, O. Kitao, H. Nakai, T. Vreven, K. Throssell, J. A. Montgomery Jr, J. E. Peralta, F. Ogliaro, M. J. Bearpark, J. J. Heyd, E. N. Brothers, K. N. Kudin, V. N. Staroverov, T. A. Keith, R. Kobayashi, J. Normand, K. Raghavachari, A. P. Rendell, J. C. Burant, S. S. Iyengar, J. Tomasi, M. Cossi, J. M. Millam, M. Klene, C. Adamo, R. Cammi, J. W. Ochterski, R. L. Martin, K. Morokuma, O. Farkas, J. B. Foresman and D. J. Fox, *Gaussian 16, Rev. C.01*, Wallingford, CT, 2016.

33 X.-S. Wu, X.-L. Dong, B.-Y. Wang, J.-L. Xia and W.-C. Li, Revealing the sodium storage behavior of biomass-derived hard carbon by using pure lignin and cellulose as model precursors, *Renewable Energy*, 2022, **189**, 630–638.

34 D. Kim, K. Yoshikawa and K. Park, Characteristics of biochar obtained by hydrothermal carbonization of cellulose for renewable energy, *Energies*, 2015, **8**(12), 14040–14048.

35 N. Karikalan, M. Velmurugan, S. M. Chen and C. Karuppiah, Modern approach to the synthesis of $Ni(OH)_2$ decorated sulfur doped carbon nanoparticles for the nonenzymatic glucose sensor, *ACS Appl. Mater. Interfaces*, 2016, **8**(34), 22545–22553.

36 H. A. Wu, Y. Zhu, S. W. Bian, J. H. Ko, S. F. Y. Li and Q. Y. Xu, H_2S adsorption by municipal solid waste incineration (MSWI) fly ash with heavy metals immobilization, *Chemosphere*, 2018, **195**, 40–47.

37 J. Hong, J. Y. Xie, S. Mirshahghassemi and J. Lead, Metal (Cd, Cr, Ni, Pb) removal from environmentally relevant waters using polyvinylpyrrolidone-coated magnetite nanoparticles, *RSC Adv.*, 2020, **10**(6), 3266–3276.

38 K. A. Krishnan, K. G. Sreejalekshmi and R. S. Baiju, Nickel(II) adsorption onto biomass based activated carbon obtained from sugarcane bagasse pith, *Bioresour. Technol.*, 2011, **102**(22), 10239–10247.

39 G. Sciortino, N. Lihi, T. Czine, J.-D. Maréchal, A. Lledós and E. Garribba, Accurate prediction of vertical electronic transitions of Ni(II) coordination compounds via time dependent density functional theory, *Int. J. Quantum Chem.*, 2018, **118**(16), e25655.

40 M. Lukács, D. Csilla Pálinkás, G. Szunyog and K. Várnagy, Metal binding ability of small peptides containing cysteine residues, *ChemistryOpen*, 2021, **10**(4), 451–463.

41 Y. Wang, J. E. Panzik, B. Kiefer and K. K. Lee, Crystal structure of graphite under room-temperature compression and decompression, *Sci. Rep.*, 2012, **2**, 520.

42 V. Choudhary, S. I. Sandler and D. G. Vlachos, Conversion of xylose to furfural using Lewis and Brønsted acid catalysts in aqueous media, *ACS Catal.*, 2012, **2**(9), 2022–2028.

43 Y. Liu, C. Ma, C. Huang, Y. Fu and J. Chang, Efficient conversion of xylose into furfural using sulfonic acid-functionalized Metal-Organic Frameworks in a biphasic system, *Ind. Eng. Chem. Res.*, 2018, **57**(49), 16628–16634.